Journal of Applied Fluid Mechanics, Vol. 9, No. 2, pp. 999-1011, 2016.
Available online at www.jafmonline.net, ISSN 1735-3572, EISSN 1735-3645.
DOI: 10.18869/acadpub.jafm.68.225.22696

On Efficient Spectral Perturbation Method for Unsteady Boundary-Layer Flows Caused by an Impulsively Stretching Plate

S. S. Motsa

School of Mathematics, Statistics and Computer Science, University of KwaZulu-Natal, Private Bag X01, Scottsville 3209, Pietermaritzburg, South Africa

Corresponding Author Email:sandilemotsa@gmail.com

(Received January 18, 2014; accepted March 16, 2015)

ABSTRACT

This investigation extends prior work on the use of perturbation techniques in the solution of unsteady boundary layer flows caused by an impulsively stretching sheet. We propose a spectral method based approach to solve the governing sequence of differential equations generated by the perturbation series approximation. The aim of this study is to demonstrate that, in contrast to conclusions drawn from previous research on this subject, the perturbation approach can be used efficiently to obtain very accurate solutions that are valid on the whole problem domain, in both dimensionless space ($0 \le \eta < \infty$) and time ($0 \le \tau < \infty$). The applicability of the proposed method, herein after referred to as the spectral perturbation method (SPM), is tested, respectively, on systems of one, two and three previously reported nonlinear partial differential equations that model different versions of unsteady boundary layer flow problems. A residual error analysis is conducted in order to assess the accuracy of the present method. Computational efficiency of the method is demonstrated by comparing with results obtained using the Keller-Box method.

Keywords: Chebychev spectral collocation; Perturbation method; Unsteady boundary layer; Keller-box.

1. INTRODUCTION

Boundary layer flows of an incompressible fluid over a stretching surface are one of the classical problems of fluid mechanics with both theoretical and practical value. There is a large volume of published literature describing the important engineering applications of such flows. Examples include aerodynamic extrusion of plastic sheets, the cooling process of metallic plates in a cooling bath, the cooling and/or drying of paper and textiles, etc. In the special case where the unsteady boundary layer is due to an impulsively started flat plate, various forms of the governing equations have been considered by some researchers using both analytical and numerical approaches which have advantages and drawbacks.

The equations governing the unsteady boundary layer flows due to an impulsively stretching surface in a viscous fluid constitute a system of nonlinear partial differential equations defined on a semi-infinite domain in both space and time. Williams and Rhyne (1980) introduced a very convenient transformation of converting the infinite time scale of unsteady problems to a finite region of integration. In recent years, there has been an increasing amount of literature on the solution of the unsteady boundary layer flows that employs the Williams and Rhyne (1980) transformation. These studies include the work of Seshadri (2002) who used the Keller-box method of (Cebeci and Bradshaw 1984) and a perturbation series approach for the solution of unsteady mixed convection flow along a heated vertical plate. Gorvadhan and Kishan (2012) solved a related unsteady problem of micropolar fluid over a stretching sheet numerically using the Adams-Predictor Corrector method. Nazar and Pop 2004a; R. Nazar and Pop 2004b solved the unsteady boundary-layer flow problem due to an impulsively stretching surface in a rotating fluid by means of the Keller-box numerical method, and they obtained a first-order perturbation approximation of the solution.

A serious drawback of the perturbation approach is that it gives solutions that are only valid for small time. Liao (2006) presented an alternative analytical approach, based on the so-called homotopy analysis method (HAM) that was meant to address some of the limitations of the perturbation methods by offering solutions that are uniformly valid for all time. Inspired by the promise of Liao's HAM (Liao 2006), many researchers have adopted the HAM approach as a tool for solving unsteady boundary

layer problems (see, for example Ali 2008; I. Ahmad and Ayub 2008; T. Hayat and Abbas 2010; Kumari and Nath 2009; A. Mehmood and Shah 2008a; A. Mehmood and Shah 2008b;S. Nadeem and Khan 2010; M. Sajid and Ayub 2008;M. Sajid 2009; Y. Tan and Liao 2007; H. Xu and Pop2006; Xu and Pop 2008)). In the framework of the

HAM, the nonlinear PDEs describing the unsteady boundary layer flow are reduced to an infinite number of linear ordinary differentials equations which are governed by an auxiliary linear operator that can be varied to improve the accuracy of the method. As pointed out by (Liao 2006), one of the attractive features of the HAM is that is offers flexibility in the choice of initial approximation and linear operator which can are carefully selected to ensure that the higher order perturbation equations can be integrated analytically. This is in sharp contrast to small parameter perturbation methods whose higher order perturbation equations are impossible to solve analytically beyond the first order approximation in unsteady similarity boundary layer flow problems. The observation made in previous studies that employ the perturbation approach (Liao 2006; Nazar and Pop 2004a; Nazar and Pop 2004b; R. Seshadri 2002) in the solution of unsteady boundary-layer flows is that it is impossible to obtain analytical solutions which are valid for all time. The perturbation approach only yields first order approximate solutions. Makukula and Motsa (2014) used the numerical version of the HAM, called the Spectral homotopy analysis method (SHAM) to solve the Von Karman equations under the Williams and Rhyne (1980) transformation. Like the HAM, the SHAM also depends on convergence controlling parameters. The process of seeking the optimal value of the convergence controlling parameter first before the problem is solved may lead to inefficiency in these methods.

In this study, we present a spectral method approach that overcomes the limitations of the analytic attempts for solving higher order perturbation equations for unsteady boundary layer flow equations. We employ the Chebyshev pseudo spectral method to gain numerical approximate solution of the higher order perturbation equations which are impossible to use analytically. We demonstrate that using spectral method to integrate the perturbation equations results in very accurate solutions that are uniformly valid in the whole time domain $0 \le \tau < \infty$. To demonstrate the applicability of the proposed method, hereinafter referred to as the Spectral Perturbation Method (SPM), we consider three previously reported models defined by coupled systems of one, two, and three nonlinear PDEs. The accuracy of the SPM is validated against results generated using the popular Keller-box implicit finite difference method. The numerical results demonstrate that the proposed method is highly accurate and significantly more computationally efficient than the Keller-box method. Unlike other numerical methods the proposed method solves a partial differential equation by only applying discretization only in the space direction. This results in significant computation timesaving.

The rest of the paper is organized as follows. Section2 details the governing nonlinear PDEs that are used for numerical experimentation in this work. In Section3 we give a brief introduction to the Chebyshev spectral collocation method and describe the idea of blending it with the perturbation series equations for all the model unsteady boundary layer equations under investigation. Section 4 presents the results and discussion. Conclusions are given in Section 5.

2. GOVERNING NONLINEAR PARTIAL EQUATIONS

In this section we give the nonlinear partial differential equations that describe the different types of unsteady boundary layer flows under investigation. In order to properly assess the capacity of the proposed method of solution, we consider three different types of nonlinear PDEs with different complexities.

2.1 Unsteady Boundary-Layer Flows Caused by an Impulsively Stretching Plate

The governing partial differential equations can be obtained by using the standard stream function formulation in conjunction with the transformations suggested by Williams and Rhyne (1980). The dimensionless governing equation is obtained (see

(Liao 2006; Nazar and Pop 2004b; R. Seshadri

2002) for details) as

$$\frac{\partial^3 f}{\partial \eta^3} + \frac{1}{2}(1-\xi)\eta\frac{\partial^2 f}{\partial \eta^2} + \xi\left[f\frac{\partial^2 f}{\partial \eta^2} - \left(\frac{\partial f}{\partial \eta}\right)^2\right] = \xi(1-\xi)\frac{\partial^2 f}{\partial \xi \partial \eta}, \quad (1)$$

subject to the boundary conditions

$$f(0,\xi) = 0, \quad \left.\frac{\partial f}{\partial \eta}\right|_{\eta=0} = 1, \quad \left.\frac{\partial f}{\partial \eta}\right|_{\eta\to+\infty} = 0, \quad (2)$$

where $\xi \in [0,1]$ is the dimensionless time-scale defined as

$$\xi = 1 - e^{-\tau}, \quad \tau = bt, \quad (3)$$

with b a positive constant and t is the time variable. We remark that the transformations (3) are used to convert the original time scale $0 \le \tau < \infty$ to the finite scale $0 \le \xi \le 1$.

In the analysis of boundary layer flow problems, a quantity that is of physical interest is the skin friction which, in this model, is given(Liao 2006; Nazarand Pop 2004b; Seshadri 2002), in dimensionlessform, as

$$C_f Re_x^{1/2} = \xi^{-1/2} f''(\xi, 0), \quad (4)$$

Where Re_x is the local Reynolds number.The initial unsteady solution at $\xi = 0$ ($\tau = 0$) for the governing equation (1) is obtained as a solution of the equation

$$f''' + \frac{1}{2}\eta f'' = 0,$$
$$f(0,0) = 0, \quad f'(0,0) = 1, \quad f'(\infty,0) = 0, \tag{5}$$

where the primes denote differentiation with respect to η. Solving (5) gives

$$f(\eta,0) = \eta erfc(\eta/2) + \frac{2}{\sqrt{\pi}}[1 - \exp(-\eta^2/4)] \tag{6}$$

where erfc (η) is the standard complementary error function defined by

$$erfc(\eta) = \frac{2}{\sqrt{\pi}}\int_{\eta}^{\infty} \exp(-z^2)dz \tag{7}$$

2.2 Unsteady Boundary Layer Flow Due to Stretching Surface in a Rotating Fluid

In this section we consider the problem of unsteady flow due to a stretching surface in a rotating fluid. The governing equations are given in Nazar and Pop (2004b) in dimensionless form as

$$f''' + \frac{1}{2}(1-\xi)\eta f'' + \xi\left(ff'' - f'^2 + 2\lambda h\right) = \xi(1-\xi)\frac{\partial f'}{\partial \xi}, \tag{8}$$

$$h'' + \frac{1}{2}(1-\xi)\eta h' + \xi\left(fh' - f'h - 2\lambda f'\right) = \xi(1-\xi)\frac{\partial h}{\partial \xi}, \tag{9}$$

subject to

$$f(0,\xi) = 0, \quad f'(0,\xi) = 1, \quad h(0,\xi) = 0,$$
$$f'(\infty,\xi) = 0, \quad h(\infty,\xi) = 0 \tag{10}$$

where $f(\eta,\xi)$ and $h(\eta,\xi)$ are velocity components and λ is the dimensionless angular velocity and the primes denote differentiation with respect to the variable η. The initial unsteady solution at $\xi = 0$, in obtained by setting $\xi = 0$ and substituting in equations (8 - 10). The resulting equations admit the following exact analytical solutions

$$f(\eta,0) = \eta erfc\left(\frac{\eta}{2}\right) + \frac{2}{\sqrt{\pi}}\left[1 - \exp\exp\left(-\frac{\eta^2}{4}\right)\right],$$
$$h(\eta,0) = 0. \tag{11}$$

The non-dimensional skin friction coefficients in and directions, C_f^x and C_f^y, are given (Nazar and Pop 2004b) as

$$C_f^x Re_x^{\frac{1}{2}} = \xi^{-\frac{1}{2}} f''(0,\xi), \quad C_f^y Re_x^{\frac{1}{2}} = \xi^{-\frac{1}{2}} h'(0,\xi), \tag{12}$$

where Re_x is the local Reynolds number.

2.3 Unsteady Boundary Layer Flow Due to Stretching Surface in a Rotating Fluid

We consider the boundary layer flow of unsteady three-dimensional flow and heat transfer on a stretching surface in the presence of of a magnetic field. The governing equations can be expressed in dimensionless form as(Kumari and Nath 2009)

$$f''' + \frac{1}{2}(1-\xi)\eta f'' + \xi\left[(f+s)f'' - f'^2 - Mf'\right] = \xi(1-\xi)\frac{\partial f'}{\partial \xi}, \tag{13}$$

$$s''' + \frac{1}{2}(1-\xi)\eta s'' + \xi\left[(f+s)s'' - s'^2 - Ms'\right] = \xi(1-\xi)\frac{\partial s'}{\partial \xi}, \tag{14}$$

$$g'' + \frac{1}{2}\Pr(1-\xi)\eta g' + \Pr\xi(f+s)g' = \Pr\xi(1-\xi)\frac{\partial g}{\partial \xi}, \tag{15}$$

subject to the boundary conditions

$$f(0,\xi) = s(0,\xi) = 0, \; f'(0,\xi) = 1,$$
$$s'(0,\xi) = c, \quad g(0,\xi) = 1, \tag{16}$$

$$f'(\infty,\xi) = s'(\infty,\xi) = g(\infty,\xi) = 0, \tag{17}$$

where f', s' are dimensionless velocities, g is the dimensionless temperature, Pr is the Prandtl number, c is the stretching ratio and M is the magnetic parameter.

The initial unsteady solution can be found exactly by setting $\xi = 0$ in the above equations and solving the resulting equations. The closed form analytical solutions are given as (Kumari and Nath 2009),

$$g(\eta,0) = erfc\left(\frac{\sqrt{\Pr}\eta}{2}\right), \; f(\eta,0) = c^{-1}s(\eta,0) = \eta erfc(\eta/2) + \frac{2}{\sqrt{\pi}}[1 - \exp(-\eta^2/4)], \tag{18}$$

The local skin friction coefficients in x - and y - directions and the local Nusselt number can be expressed as

$$C_f^x Re_x^{\frac{1}{2}} = -\xi^{-\frac{1}{2}} f''(0,\xi), \quad C_f^y Re_y^{\frac{1}{2}} = -\xi^{-\frac{1}{2}} s''(0,\xi),$$
$$Nu_x Re_x^{-\frac{1}{2}} = -\xi^{-\frac{1}{2}} g'(0,\xi), \tag{19}$$

where Re_x and Re_y are local Reynolds numbers, C_f^x and C_f^y are the local skin friction coefficients

in x - and y - directions, respectively, Nu_x is the local Nusselt number, $f''(0,\xi)$ and $s''(0,\xi)$ are the surface shear stresses in x - and y -directions, respectively, $g'(0,\xi)$ is the surface heat transfer parameter.

3. SPECTRAL PERTURBATION METHOD

In this section we introduce the proposed spectral perturbation method (SPM) that is used as a solution method for the problems described in the previous section.In the region $0<\xi<1$ ($0\le\tau<\infty$) there is no exact analytical solution to any of the governing nonlinear PDEs described above. For example, Seshadri (2002) and Nazar and Pop (2004b) sought series solutions of the governing equation (1) of the form

$$f(\eta,\xi)=f_0(\eta)+f_1(\eta)\xi+f_2(\eta)\xi^2+\ldots, \qquad (20)$$

by regarding ξ as a small parameter. Using this series approach, only the first order perturbation was reported in these studies. The analytical approach is not viable because higher order solutions are impossible to obtain analytically. Below, we demonstrate that, for the unsteady boundary layer flow problems, the perturbation approach can be used to give exceedingly accurate results in an very efficient manner when the integration in the space direction η is done numerically using spectral methods.

3.1 Spectral Perturbation Method Solution for Example (1)

Following, Liao (2006), Nazar and Pop (2004b), and Seshadri (2002), we regard ξ as a small parameter to search for a perturbation approximation in the form

$$f(\eta,\xi)=\sum^{k=0+\infty} f_k(\eta)\xi^k. \qquad (21)$$

Substituting (21) in the governing equation (1) and balancing coefficients of equal power of ξ, we obtain,

$$f'''_0+\frac{\eta}{2}f''_0=0,$$

$$f_0(0)=0,\quad f'_0(0)=1,\quad f'_0(\infty)=0, \qquad (22)$$

$$f'''_k+\frac{\eta}{2}f''_k-kf'_k=\frac{\eta}{2}f''_{k-1}-(k-1)f'_{k-1}$$

$$-\sum_{i=0}^{k-1}\left[f_i f_{k-i-1}''-f_i' f_{k-i-1}'\right], \qquad (23)$$

$$f_k(0)=0,\quad f'_k(0)=0,\quad f'_k(\infty)=0, k\ge 1. \qquad (24)$$

In order to apply the spectral method in an accurate and efficient manner, in solving equation (23), it is convenient to reduce the order of the differential equation from three to two. To this end, we introduce the variable $u=f'$ and substitute in (23) to obtain,

$$u''_k+\frac{\eta}{2}u'_k-ku_k=\frac{\eta}{2}u'_{k-1}-(k-1)u_{k-1}$$

$$-\sum_{i=0}^{k-1}\left[f_i u_{k-i-1}'-u_i u_{k-i-1}\right], \qquad (25)$$

$$u_k(0)=0,\quad u_k(\infty)=0,\quad k\ge 1 \qquad (26)$$

$$f'_k=u_k,\quad f_k(0)=0. \qquad (27)$$

The solution to equation (22) is the initial unsteady flow solution given by equation (6). Starting from a known f_0 , the solutions to equations (25 - 27) can be obtained in a straightforward manner using the Chebyshev spectral collocation method since the governing equations are a sequence of linear ordinary differential equations. Because a spectral method is used to integrate the perturbation differential equations, the method is referred to as the spectral perturbation method (SPM) in this study. Below, we give a brief description of the spectral method used in the solution of equations of the form (25).

Numerical methods such as finite differences, finite element method, spectral method and many others can be used to solve equations of the form (25). Spectral methods, such as the Chebyshev pseudo-spectral method, been found to be very convenient tools for ordinary differential equations with variable coefficients. Spectral methods are now becoming the preferred tools for solving ordinary and partial differential equations because of their elegance and high accuracy in resolving problems with smooth functions.

For brevity, we omit the details of the spectral methods, and refer interested readers to Canuto et. al. (1988) and Trefethen (2000). Before applying the spectral method, it is convenient to transform the domain on which the governing equation is defined to the interval [-1,1] where the spectral method can be implemented. For the convenience of the numerical computations, the semi-infinite domain in the space direction is approximated by the truncated domain $[0,\eta_\infty]$, where η_∞ is a finite number selected to be large enough to represent the behaviour of the flow properties when η is very large. We use the transformation $\eta=\eta_\infty(Y+1)/2$ to map the interval $[0,\eta_\infty]$ to [-1,1]. The basic idea behind the spectral collocation method is the introduction of a differentiation matrix D which is used to approximate the derivatives of the unknown variables $f(\eta)$ at the collocation points (grid points) as the matrix vector product

$$\frac{dF}{d\eta}=\sum_{k=0}^{N_x} D_{lk}f(\eta_k)=DF,\quad l=0,1,\ldots,N_x \qquad (28)$$

where N_x+1 is the number of collocation points, $D=2D/\eta_\infty$, and $F=[f(Y_0),f(Y_1),\ldots,f(Y_{N_x})]^T$ is the vector function at the collocation points. Higher order derivatives are obtained as powers of D, that is

$$F^{(p)}=D^pF. \tag{29}$$

where p is the order of the derivative. We choose the Gauss-Lobatto collocation points to define the nodes in [-1,1] as

$$Y_j=\cos\left(\frac{\pi j}{N_x}\right), j=0,1,\ldots,N_x. \tag{30}$$

The matrix D is of size $(N_x+1)\times(N_x+1)$ and its entries are defined (Canuto et. al. 1998; Trefethen 2000) as

$$\begin{aligned} D_{jk} &= \frac{c_j}{c_k}\frac{(-1)^{j+k}}{Y_j-Y_k}\ j\neq k;\ j,k=0,1,\ldots,N_x,\\ D_{kk} &= -\frac{Y_k}{2(1-Y_k^2)}\ k=1,2,\ldots,N_x-1, \\ D_{00} &= \frac{2N^2+1}{6}=-D_{N_xN_x}, \end{aligned} \tag{31}$$

With

$$c_k=\begin{cases}2 & k=0,N_x\\ 1 & -1\le k\le N_x-1\end{cases} \tag{32}$$

Applying the Chebyshev spectral collocation method on equations (25 -27) gives

$$AU_k=B_{k-1}, u_k(\eta_{N_x})=0, u_k(\eta_0)=0, \tag{33}$$

$$DF_k=U_k,\quad f_k(\eta_{N_x})=0, \tag{34}$$

where

$$A=D^2+\frac{\eta}{2}D-kI$$

with I being an $(N_x+1)\times(N_x+1)$ identity matrix and $\bar{\eta}$ is a diagonal matrix obtained from the vector $[\eta_0,\eta_1,\ldots,\eta_{N_x}]$. The vector $\bar{B}_{k-1}$ is generated by evaluating the right hand side of equation (25) at the collocation points η_j with the derivatives replaced by spectral differentiation matrices. The boundary conditions are imposed on the first and last rows of $\bar{A},\bar{B}$ and D. Thus, starting from a known U_0, the solutions U_k, $k\ge 1 U_k$ can be obtained as

$$U_k=\bar{A}^{-1}\bar{B}_{k-1},\quad F_k=D^{-1}U_k, \tag{35}$$

where

$F_k=[f_k(\eta_0),f_k(\eta_1),\ldots,f_k(\eta_{N_x})]^T$,

$U_k=[u_k(\eta_0),u_k(\eta_1),\ldots,u_k(\eta_{N_x})]^T$.

3.2 Spectral Perturbation Method Solution for Example (8-9)

To solve the governing equations (8-9) we search for a perturbation approximation of the form

$$f(\eta,\xi)=\sum_{k=0}^{+\infty}f_k(\eta)\xi^k \quad h(\eta,\xi)=\sum_{k=0}^{+\infty}h_k(\eta)\xi^k \tag{36}$$

Substituting (36) in the governing equations (8-9) and balancing terms of equal order of ξ gives

$$f'''_0+\frac{\eta}{2}f''_0=0,\ f_0(0)=0, \tag{37}$$

$$f'_0(0)=1,\ f'_0(\infty)=0,$$

$$h''_0+\frac{\eta}{2}h'_0=0, h_0(0)=0, h_0(\infty)=0, \tag{38}$$

$$f'''_k+\frac{\eta}{2}f''_k-kf'_k=\frac{\eta}{2}f'_{k-1}-(k-1)f_{k-1}'$$

$$-2\lambda h_{k-1}-\sum^{i=0k-1}{}'[f_if_{k-i-1}'-f_{i'}f_{k-i-1}'], \tag{39}$$

$$f_k(0)=0,\ f'_k(0)=0,\ f'_k(\infty)=0, k\ge 1. \tag{40}$$

$$h''_k+\frac{\eta}{2}h'_k-kh_k=\frac{\eta}{2}h'_{k-1}-(k-1)h_{k-1}$$

$$+2\lambda f'_{k-1}-\sum_{i=0}^{k-1}{}'[f_ih_{k-i-1}'-f_ih_{k-i-1}], \tag{41}$$

$$h_k(0)=0,\ h_k(\infty)=0\ \ k\ge 1. \tag{42}$$

We reduce the order of the highest derivative in (39) by setting $f'=u$ to obtain

$$u''_k+\frac{\eta}{2}u'_k-ku_k=\frac{\eta}{2}u'_{k-1}-(k-1)u_{k-1}$$

$$-2\lambda h_{k-1}-\sum_{i=0}^{k-1}{}'[f_iu_{k-i-1}-u_iu_{k-i-1}], \tag{43}$$

$$u_k(0)=0,\ u_k(\infty)=0,\ \ k\ge 1 \tag{44}$$

$$f'_k=u_k,\quad f_k(0)=0. \tag{45}$$

Applying the Chebyshev spectral collocation method on equations (41, 43,44) gives

$$\bar{A}U_k=\bar{B}_{1,k-1}, u_k(\eta_{N_x})=0, u_k(\eta_0)=0,$$

$$\bar{A}U_k=\bar{B}_{1,k-1},\ u_k(\eta_{N_x})=0, u_k(\eta_0)=0, \tag{46}$$

$$DF_k=U_k, f_k(\eta_{N_x})=0, \tag{47}$$

$$\bar{A}H_k=\bar{B}_{2,k-1},\ h_k(\eta_{N_x})=0,\ h_k(\eta_0)=0, \tag{48}$$

where $\bar{B}_{1,k-1}$, $\bar{B}_{2,k-1}$ are generated by evaluating the right hand side of equations (41) and (43)at the

collocation points with the derivatives replaced by spectral differentiation matrices. Thus, starting from a known U_0, H_0 the solutions U_k, $H_{k\geq 1k}$, $k\geq 1$ can be obtained as

$$U_k = \bar{A}^{-1}\,\bar{B}_{1,k-1},\; F_k = D^{-1}U_k,\; H_k = \bar{A}^{-1}\,\bar{B}_{2,\,k-1}, \tag{49}$$

where

$$H_k = [h_k(\eta_0), h_k(\eta_1), \ldots, h_k(\eta_{N_x})]^T.$$

3.3 Spectral Perturbation Method Solution for Example (13-15)

To solve the governing equations (13-15) we search for a perturbation approximation of the form

$$f(\eta,\xi) = \sum_{k=0}^{+\infty} f_k(\eta)\xi^k, s(\eta,\xi) = \sum_{k=0}^{+\infty} s_k(\eta)\xi^k,$$

$$g(\eta,\xi) = \sum_{k=0}^{+\infty} g_k(\eta)\xi^k. \tag{50}$$

Substituting (50) in the governing equations (13-15) and balancing terms of equal order of gives

$$f'''_0 + \frac{\eta}{2} f''_0 = 0,$$
$$f_0(0) = 0,\; f'_0(0) = 1,\quad f'_0(\infty) = 0, \tag{51}$$

$$s'''_0 + \frac{\eta}{2} s''_0 = 0,$$
$$s_0(0) = 0,\; s'_0(0) = c,\; s'_0(\infty) = 0, \tag{52}$$

$$g''_0 + \frac{\eta}{2}\Pr g'_0 = 0,\; g_0(0) = 1,\; g_0(\infty) = 0, \tag{53}$$

$$f'''_k + \frac{\eta}{2} f''_k - k f'_k = \frac{\eta}{2} f''_{k-1} - (k-1) f'_{k-1} + M f'_{k-1}$$

$$-\sum_{i=0}^{k-1}\left[f_i f_{k-i-1}'' + s_i f_{k-i-1}'' - f_{i'} f_{k-i-1}'\right], \tag{54}$$

$$f_k(0) = 0,\; f'_k(0) = 0,\; f'_k(\infty) = 0,\; k\geq 1, \tag{55}$$

$$s'''_k + \frac{\eta}{2} s''_k - k s'_k = \frac{\eta}{2} s''_{k-1} - (k-1) s'_{k-1} + M s'_{k-1}$$

$$-\sum_{i=0}^{k-1}\left[s_i s_{k-i-1}'' + f_i s_{k-i-1}'' - s_{i'} s_{k-i-1}'\right], \tag{56}$$

$$s_k(0) = 0,\; s'_k(0) = 0,\; s'_k(\infty) = 0,\; k\geq 1 \tag{57}$$

$$g''_k + \frac{\eta}{2}\Pr g'_k - Prk g_k = \frac{\eta}{2}\Pr g'_{k-1} - \Pr(k-1) g_{k-1}$$

$$-\Pr\sum_{i=0}^{k-1}\left[f_i g_{k-i-1} + s_i g'_{k-i-1}\right], \tag{58}$$

$$g_k(0) = 0,\; g_k(\infty) = 0 \quad k\geq 1. \tag{59}$$

To reduce the order of the highest derivatives in (54) and (56) we set $f' = u$ and $s' = w$ to obtain

$$u''_k + \frac{\eta}{2} u'_k - k u_k = \frac{\eta}{2} u'_{k-1} - (k-1) u_{k-1} + M u_{k-1}$$

$$-\sum_{i=0}^{k-1}\left[f_i u_{k-i-1}' + s_i u_{k-i-1}' - u_i u_{k-i-1}\right],$$

(60)

$$u_k(0) = 0,\; u_k(\infty) = 0,\; k\geq 1 \tag{61}$$

$$f'_k = u_k,\quad f_k(0) = 0, \tag{62}$$

$$w''_k + \frac{\eta}{2} w'_k - k w_k = \frac{\eta}{2} w'_{k-1} - (k-1) w_{k-1} + M w_{k-1}$$

$$-\sum_{i=0}^{k-1}\left[s_i w_{k-i-1}' + f_i w_{k-i-1}' - w_i w_{k-i-1}\right], \tag{63}$$

$$w_k(0) = 0,\; w_k(\infty) = 0,\quad k\geq 1 \tag{64}$$

$$s'_k = w_k,\quad s_k(0) = 0, \tag{65}$$

Applying the Chebyshev spectral collocation method on equations (58, 60,63) gives

$$\bar{A}U_k = \bar{B}_{3,k-1}, u_k(\eta_{N_x}) = 0,\; u_k(\eta_0) = 0, \tag{66}$$

$$DF_k = U_k,\quad f_k(\eta_{N_x}) = 0, \tag{67}$$

$$\bar{A}W_k = \bar{B}_{4,k-1}, w_k(\eta_{N_x}) = 0,\; w_k(\eta_0) = 0, \tag{68}$$

$$DS_k = W_k,\; s_k(\eta_{N_x}) = 0, \tag{69}$$

$$\bar{A}_1 G_k = \bar{B}_{5,k-1}, g_k(\eta_{N_x}) = 0,\quad g_k(\eta_0) = 0, \tag{70}$$

where

$$\bar{A} = D^2 + \Pr\frac{\bar{\eta}}{2} D - kPrI$$

and $\bar{B}_{3,k-1}$, $\bar{B}_{4,k-1}$, $\bar{B}_{5,k-1}$ are generated by evaluating the right hand side of equations (58), (60) and (63) at the collocation points with the derivatives replaced by spectral differentiation matrices. Thus, starting from a known U_0, F_0, W_0, S_0 and G_0 the solutions U_k, F_k, W_k, S_k and G_k, $k\geq 1$ the solutions and can be obtained, in turn, from

$$U_k = \bar{A}^{-1}\,\bar{B}_{3,k-1} F_k = D^{-1}U_k,\; W_k = \bar{A}^{-1}\,\bar{B}_{4,k-1}, \tag{71}$$

$$S_k = D^{-1}W_k,\quad G_k = \bar{A}_1^{-1}\,\bar{B}_{5,k-1}, \tag{72}$$

where

$W_k = [w_k(\eta_0), w_k(\eta_1), \ldots, w_k(\eta_{N_x})]^T$,

$S_k = [s_k(\eta_0), s_k(\eta_1), \ldots, s_k(\eta_{N_x})]^T$,

$G_k = [g_k(\eta_0), g_k(\eta_1), \ldots, g_k(\eta_{N_x})]^T$.

Insert tables and figures within your document either scattered throughout the text or all together at the end of the file. Tables and figures should be numbered consecutively, with captions below the table or figure.

4. RESULTS AND DISCUSSION

In order to determine the evolution of the boundary layer flow properties, numerical solutions of the set of governing systems of partial differential equations (1 - 2), (8 - 10) and (13 - 17) were computed using the proposed spectral perturbation method (SPM). Starting from the initial analytical solutions at $\xi = 0$ (corresponding to $\tau = 0$), the SPM series was used to generate results up to solutions near the steady state values at $\xi = 1$ (corresponding to $\tau \to \infty$). The accuracy of the computed SPM approximate results was confirmed against numerical results obtained by using the popular Keller-box implicit finite difference method as described by CEBECI. The Keller-box method is known to be accurate, fast and easier to program for boundary layer flow problems. The algorithm of the method begins with the reduction of the governing nonlinear PDEs into a system of first order equations that are discretized using central differences. The nonlinear algebraic difference equations are linearised using Newton's method and written in matrix-vector form. The linear matrix systems are solved in an efficient manner using a block-tridiagonal-elimination technique. The grid spacing in both the - and -direction is carefully selected to ensure that the Keller-box computations yield consistent results for the governing velocity and temperature distributions to a convergence level of at least 10^{-7}. On the other hand, from numerical experimentation itwasfound the $N_x = 100$ collocation points in the spectral method discretization was sufficient to give accurate results in all the governing equations and associated physical parameters used in this study. Furthermore, the finite value used to approximate the boundary conditions at infinity, was set to be $\eta_\infty = 30$ in the SPM and $\eta_\infty = 10$ in the Keller-box method. The terms of the SPM series solution were calculated until the maximum error of the residual was less than 10^{-6}. The solution that has converged to within a certain level of accuracy at the order of in the SPM approximation is denoted by

$$F(\eta_j, \xi) = \sum_{k=0}^{K} \xi^k f_k(\eta_j), \quad j = 0,1,2,\ldots,N_x. \quad (73)$$

The above expression is called the th order SPM approximate solution for $f(\eta,\xi)$, the solution of the governing partial differential equation (1). Similar expressions are used denote the SPM solutions of the other PDEs being investigated in this study (8 - 10) and (13 - 17). If the governing PDEs is

$$\mathcal{R}[f(\eta,\xi)] = 0, \quad (74)$$

where is a nonlinear operator, then the maximum error of the residual is defined as

$$Res(f) = \max_j |\mathcal{R}[F(\eta_j,\xi)]|, \quad j = 0,1,\ldots,N_x. \quad (75)$$

Table 1 shows the Keller-Box generated numerical results for the skin friction $f''(0,\xi)$ at different values of time ξ in Example (1) when $\Delta\xi = 0.002$, $\eta_\infty = 10$. A uniform grid was used and progressively refined until the results were consistent to within six decimal digits. Table 1 gives the results of the grid refinement. It can be noted from the table that results that are consistent to within 6 decimal digits were achieved when the spacing in the direction, denoted by , was 0.005. It is worth mentioning here that Keller-box method solution of equation (1) were also reported in Ali et. al (2010) where results for $f''(0,\xi)$ were tabulated for selected values of . We have opted not to compare our current results with the published results of Ali et. al (2010) because the results only agree up to 3 decimal digits. We remark, however that it was not possible to reproduce the previous results since the Keller-box parameters used to generate results and the convergence criteria used was not disclosed in Ali et. al. (2010). The grid-independence test displayed in Table 1 and the excellent agreement with the equivalent SPM results displayed in Table 2 is evidence that the present Keller-box results displayed in Table 1 are accurate to the specified number of digits.

Table 1 Keller-Box numerical values of the skin friction *-f''(0,ξ)* at different values of time ξ in Example (1) when $\Delta\xi = 0.002$, $\eta_\infty = 10$

$\xi \setminus \Delta\eta$	0.1	0.01	0.005	0.002
0.1	0.610622	0.610469	0.610468	0.610468
0.3	0.701375	0.701268	0.701267	0.701267
0.5	0.789895	0.789829	0.789828	0.789828
0.7	0.876294	0.876267	0.876267	0.876267
0.8	0.918711	0.918701	0.918701	0.918701
0.9	0.960534	0.960538	0.960538	0.960538
0.95	0.981095	0.981102	0.981102	0.981102
0.98	0.993126	0.993134	0.993134	0.993134

In Table 2, the results for the skin friction $f''(0,\xi)$ of example (1) are given for different values of time ξ. Table 2 also gives the order of the SPM approximation and the computational time required

to obtain a solution that is consistent to at least six decimal places. It can be observed from this table that converged solutions are reached at very low SPM orders when is close to zero. More terms of the series are required to give converged results when ξ is close to (as $\tau \to \infty$). However, it can be seen from the column on the run time that the desired solution is obtained after only a fraction of a second. This shows the efficiency of the proposed SPM approach in terms of the amount of time it takes the method to give the desired results. The Keller-box results and corresponding computational time are also displayed in the table. A comparison of the computational times clearly shows that there proposed SPM is exceedingly faster than the Keller-box in the computation of the solution for example (1). Consequently, it can be inferred from Table 2, that the SPM is more efficient than the Keller-box in computing an accurate solution for Example (1). It is worth mentioning that the apparent computational speed of the SPM can be explained by the fact that, unlike the Keller-box and other numerical methods, only discretization in the direction is done in the SPM algorithm. Furthermore, using spectral methods for integrating the linearised equations leads to significant saving in computation time since spectral methods require only a few grid points to yield very accurate solutions when the solution is smooth.

Table 2 Comparison between the SPM and Keller-box numerical values of the skin friction $-f''(0,\xi)$ at different values of time ξ in Example (1)

	SPM			Keller-Box	
ξ	K	$-f''(0,\xi)$	Time(s)	$-f''(0,\xi)$	Time(s)
0.1	4	0.610468	0.01	0.610468	3.96
0.3	4	0.701267	0.01	0.701267	11.45
0.5	10	0.789828	0.03	0.789828	18.78
0.7	14	0.876267	0.04	0.876266	26.17
0.8	24	0.918701	0.06	0.918701	29.88
0.9	49	0.960538	0.13	0.960538	34.05
0.95	117	0.981102	0.23	0.981102	36.52
0.98	197	0.993134	0.53	0.993134	37.98

The variation of the maximum residual error $Res(f)$ with the SPM approximation orders for Example (1) is shown in Fig. 1 at different values of time ξ. It can be seen from this figure that there is a clear trend of decreasing residual error with an increase in the order of approximation. The rate of decrease in residual error appears to be steeper for smaller values of ξ. This observation is in line with the results presented in Table 2 where it was observed that for small values of ξ, convergence to results that are accurate to within a certain level can be achieved using a few orders of the approximation method. In addition, it can be noticed in Fig. 1 that the residual error curve levels off at the fixed level below 10^{-8} for all values of ξ. From this observation we suggest that the level at which the residual curve plateaus can be used as an indicator of the maximum possible accuracy that can be achieved using the SPM with given N_x and η_∞. We remark that, in generating the data displayed in Fig. 1 changes in the values of N_x and η_∞ beyond the $N_x = 100$ and $\eta_\infty = 30$ did not significantly change the numerical results used to generate the plot.

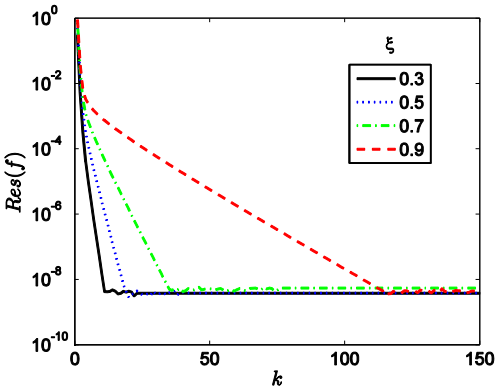

Fig. 1. Residual error curve $Res(f)$ against increasing SPM approximation orders k for Example (1) when $\xi = 0.3, 0.5, 0.7, 0.9$.

The Keller-box results for the skin frictions $f''(0,\xi)$ and $h'(0,\xi)$ corresponding to Example (8 - 10) are given in Table 3 and 4, respectively, for selected values of ξ. In this case, it was determined that a smaller step size of at least $\Delta\xi = 0.001$ was required to give accurate results to within the required six decimal digits. The results given in Table 3 and 4 were used to validate the accuracy of the SPM results.

Table 3 Keller-Box numerical values of the skin friction - $f''(0,\xi)$ at different values of time ξ in Example (8-10) when $\Delta\xi = 0.001$, $\eta_\infty = 10$

$\xi \setminus \Delta\eta$	0.1	0.01	0.005	0.002
0.1	0.614437	0.614285	0.614283	0.614283
0.3	0.736656	0.736542	0.736542	0.736541
0.5	0.890162	0.890092	0.890091	0.890091
0.7	1.074949	1.074961	1.074961	1.074961
0.8	1.175446	1.175528	1.175529	1.175529
0.9	1.268330	1.268507	1.268509	1.268509
0.95	1.297619	1.297841	1.297843	1.297844
0.98	1.306184	1.306423	1.306425	1.306426

Table 4 Keller-Box numerical values of the skin friction $-h'(0,\xi)$ at different values of time ξ in Example (8-10) when $\Delta\xi = 0.001$, $\eta_\infty = 10$

$\xi \setminus \Delta\eta$	0.1	0.01	0.005	0.002
0.1	0.112439	0.112403	0.112402	0.112402
0.3	0.331979	0.331864	0.331863	0.331863
0.5	0.536084	0.535901	0.535900	0.535899
0.7	0.707314	0.707101	0.707099	0.707099
0.8	0.769329	0.769122	0.769120	0.769120
0.9	0.803207	0.803018	0.803016	0.803016
0.95	0.810059	0.809875	0.809874	0.809874
0.98	0.825332	0.825139	0.825137	0.825137

Tables 5 and 6 give a comparisonof the SPM and Keller-box results for the skin frictions $f''(0,\xi)$ and $h'(0,\xi)$, respectively, for Example (8 - 10) when $\lambda = 1$. The minimum order of the SPM approximation (K) required to give results that are consistent to six decimal digits as well as the run time is also displayed in the table. The trend that can be observed from this table is that few terms of the SPM are required to obtain converged results when is small and significantly more terms are required when ξ is close to 1. However, the computational time needed to achieve this level of convergence is still reasonably small when the total number of terms used are considered. The Keller-box results given in Tables 5 and 6 were calculated using non-uniform step size in the -direction and a uniform step size $\Delta\xi = 0.001$ in the -direction. Using a non-uniform grid size significantly improves the computation time of the Keller-box method. Thus, to speed up the computation times for the Keller-box method, computations were carried out with an initial step size of $\Delta\eta_0 = 0.001$. This was gradually increased by the variable grid parameter (VGP) factor of 1.005 between successive grid points in accordance with the formula $\eta_j = \eta_{j-1} + VGP \times \Delta\eta_{j-1}$ for $j = 1,2,\ldots,J$ (where J is the number of grid points in the direction). It can be seen from Tables 5 and 6 that the numerical values of the skin frictions computed using the SPM and Keller-box numerical approach are in good agreement. However, there is a substantial difference in the computation times of the too methods. Again, the SPM is observed to be must faster than the Keller-box method. Also, the number of SPM series terms required to give the 6 decimal digits converged results is increases with an increase in ξ. Notwithstanding this apparent slower convergence when $\xi \to 1$, the SPM eventually converges fully to the required level of accuracy within a reasonably short time. This demonstrates the efficiency of the proposed SPM approach in solving the governing model PDEs. The convergence speed of the SPM and, in turn, the computational cost can further be improved by using Padé approximates.

Table 5 Comparison between the SPM and Keller-box numerical values of the skin friction $-f''(0,\xi)$ at different values of time ξ in Example (8-10) when $\lambda = 1$

	SPM			Keller-Box	
ξ	K	$-f''(0,\xi)$	Time(sec)	$-f''(0,\xi)$	Time(sec)
0.1	4	0.614283	0.045	0.614283	19.04
0.3	9	0.736541	0.049	0.736542	57.11
0.5	16	0.890091	0.086	0.890091	96.20
0.7	27	1.074961	0.207	1.074961	135.34
0.8	41	1.175529	0.321	1.175529	154.88
0.9	91	1.268509	0.701	1.268509	174.73
0.95	163	1.297842	1.585	1.297843	187.71
0.98	422	1.306426	4.886	1.306425	195.31

Table 6 Comparison between the SPM and Keller-box numerical values of the skin friction $-h'(0,\xi)$ at different values of time ξ in Example (8-10) when $\lambda = 1$

	SPM			Keller-Box	
ξ	K	$h'(0,\xi)$	Time(sec)	$h'(0,\xi)$	Time(sec)
0.1	7	0.112402	0.045	0.112402	19.04
0.3	9	0.331863	0.049	0.331863	57.11
0.5	16	0.535899	0.086	0.535899	96.20
0.7	35	0.707099	0.207	0.707099	135.34
0.8	48	0.769120	0.321	0.769120	154.88
0.9	79	0.803015	0.701	0.803016	174.73
0.95	190	0.809873	1.585	0.809874	187.71
0.98	397	0.825143	4.886	0.825137	195.31

Fig. 2 shows the maximum residual errors for f and h respectively, against increasing orders of the SPM approximation in Example (8 - 10). From the graphs, it can seen that the residual errors decrease sharply with an increase in the order of approximation. We observe, also, that the residual curves tend to plateau at more or less a fixed level for the different values of ξ considered. The interpretation of this result is that the proposed method will converge up to a certain saturation level which is equal to the level at which the curves level off. The saturation level is at least 10^{-12} in the equation for $f(\eta,\xi)$ and about 10^{-12} in the equation for $h(\eta,\xi)$. We also note that as gets closer to ξ (τ -) the plateau is reached at a higher order of approximation. This is typical of perturbation based methods which are well known to be accurate when the series expansion is about a small parameter. In the case of the SPM, it is interesting to observe that even when ξ (τ -), very accurate results can still be obtained, albeit with a higher order of approximation.

In Tables 7 - 9 the Keller-box-calculated results for

the reduced skin frictions and surface heat transfer rate ($f''(0,\xi)$ $s''(0,\xi)$, $g(0,\xi)$) at different time levels are are given for $\Pr = 0.7, c = 0.5, M = 1$. A uniform grid with a step-size of $\Delta\xi = 0.002$ was used to compute the approximate results. The step-size in the -direction was gradually reduced until the results were consistent to at least six decimal digits. The converged results were used to validate the accuracy of the SPM as shown in Tables 10-12.

Table 7 Keller-Box numerical values of the skin friction $-f''(0,\xi)$ at different values of time ξ in Example (13-17) when $\Delta\xi = 0.002$, $\eta_\infty = 10$

$\xi \setminus \Delta\eta$	0.1	0.01	0.002	0.001
0.1	0.674624	0.674445	0.674443	0.674443
0.3	0.880598	0.880409	0.880407	0.880407
0.5	1.069127	1.068931	1.068930	1.068929
0.7	1.242261	1.242069	1.242067	1.242067
0.8	1.323620	1.323434	1.323432	1.323432
0.9	1.401778	1.401600	1.401598	1.401598
0.95	1.439718	1.439544	1.439543	1.439543
0.98	1.462134	1.461963	1.461961	1.461961

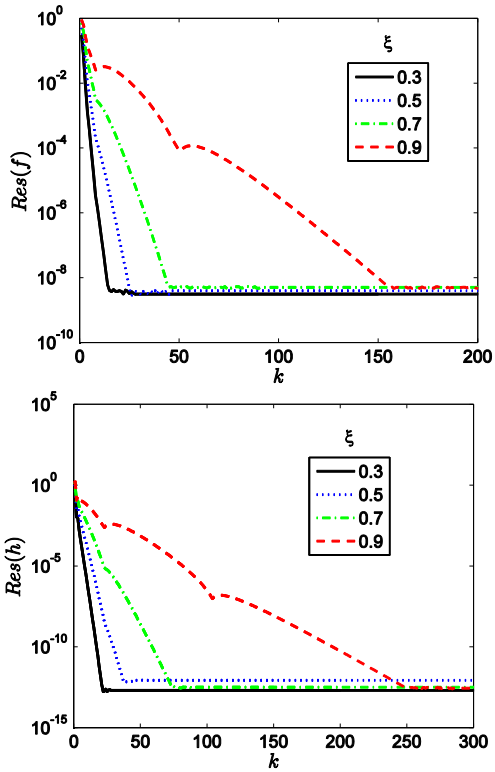

Fig. 2. Residual error curves $Res(f)$ and $Res(h)$ against increasing SPM approximation orders k for Example (8 - 10) when $\lambda = 1$.

Table 8 Keller-Box numerical values of the skin friction $-s''(0,\xi)$ at different values of time ξ in Example (13-17) when $\Delta\xi = 0.002$, $\eta_\infty = 10$

$\xi \setminus \Delta\eta$	0.1	0.01	0.002	0.001
0.1	0.327681	0.327586	0.327585	0.327585
0.3	0.414675	0.414566	0.414565	0.414565
0.5	0.496494	0.496371	0.496369	0.496369
0.7	0.573360	0.573226	0.573224	0.573224
0.8	0.610013	0.609875	0.609873	0.609873
0.9	0.645527	0.645384	0.645383	0.645383
0.95	0.662870	0.662726	0.662724	0.662724
0.98	0.673150	0.673005	0.673003	0.673003

Table 9 Keller-Box numerical values of the surface heat transfer rate $-g'(0,\xi)$ at different values of time ξ in Example (13-17) when $\Delta\xi = 0.001$, $\eta_\infty = 10$

$\xi \setminus \Delta\eta$	0.1	0.01	0.005	0.002
0.1	0.483188	0.483086	0.483085	0.483085
0.3	0.503602	0.503506	0.503506	0.503505
0.5	0.521105	0.521022	0.521021	0.521021
0.7	0.534131	0.534065	0.534065	0.534064
0.8	0.537730	0.537674	0.537674	0.537674
0.9	0.537175	0.537130	0.537130	0.537130
0.95	0.533135	0.533094	0.533094	0.533094
0.98	0.526807	0.526767	0.526767	0.526767

Table 10 Comparison between the SPM and Keller-box numerical values of the skin friction $-f''(0,\xi)$ at different values of time ξ for Example (13-17) when $\Pr = 0.7$, $c = 0.5, M = 1$

	SPM			Keller-Box	
ξ	K	$-f''(0,\xi)$	Time(sec)	$-f''(0,\xi)$	Time(sec)
0.1	5	0.674443	0.082	0.674444	22.644
0.3	7	0.880407	0.136	0.880408	65.809
0.5	8	1.068930	0.154	1.068930	109.886
0.7	9	1.242067	0.214	1.242068	157.737
0.8	13	1.323432	0.235	1.323432	186.486
0.9	24	1.401598	0.611	1.401598	215.769
0.95	60	1.439543	1.180	1.439543	230.240
0.98	51	1.461961	3.623	1.461962	238.769

Table 11 Comparison between the SPM and Keller-box numerical values of the skin friction $-s''(0,\xi)$ at different values of time ξ for Example (13-17) when $\Pr = 0.7, c = 0.5, M = 1$

	SPM			Keller-Box	
ξ	K	$s''(0,\xi)$	Time(sec)	$s''(0,\xi)$	Time(sec)
0.1	5	0.327586	0.082	0.327586	22.644
0.3	6	0.414565	0.136	0.414565	65.809
0.5	7	0.496369	0.154	0.496370	109.886
0.7	8	0.573224	0.214	0.573224	157.737
0.8	11	0.609873	0.235	0.609873	186.486
0.9	23	0.645383	0.611	0.645383	215.769
0.95	30	0.662724	1.180	0.662725	230.240
0.98	52	0.673003	3.623	0.673003	238.769

Table 12Comparison between the SPM and Keller-box numerical values of the surface heat transfer rate $g'(0,\xi)$ at different values of time ξ for Example (13-17) when

$\Pr = 0.7,\ c = 0.5, M = 1$

	SPM			Keller-Box	
ξ	K	$-g'(0,\xi)$	Time(sec)	$-g'(0,\xi)$	Time(sec)
.1	5	0.483085	0.082	0.483086	22.644
.3	9	0.503505	0.136	0.503506	65.809
.5	12	0.521021	0.154	0.521021	109.886
.7	29	0.534064	0.214	0.534065	157.737
.8	33	0.537674	0.235	0.537674	186.486
.9	67	0.537130	0.611	0.537130	215.769
.95	133	0.533094	1.180	0.533094	230.240
.98	275	0.526767	3.623	0.526766	238.769

Tables 10, 11 and 12 give the results for the reduced skin frictions ($f''(0,\xi)$, $s''(0,\xi)$) and surface heat transfer rate $g(0,\xi)$, respectively. The tables gives a comparison between the SPM and Keller-box run times required to give six-decimal digit consistent solutions are given when $\Pr = 0.7, c = 0.5, M = 1$. Again, it can be observed that the SPM is significantly faster than the Keller-box method in terms of computational time. The two results are in good agreement for all values of ξ considered. The trends displayed in Tables 10 - 12 accords with the earlier observations made in Tables 2, 5 and 6. In particular, it can be seen from the table that only a few terms of the SPM approximation are required to give converged results when ξ is small and a higher order of approximation required is higher when ξ is closer to 1.

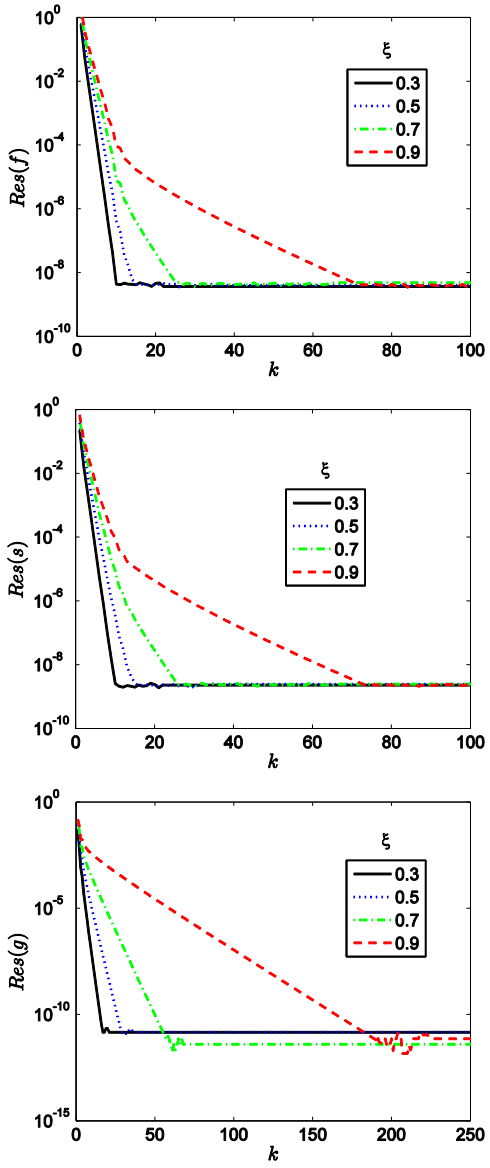

Fig. 3. Residual error curves $Res(f)$, $Res(s)$ and $Res(g)$ against increasing approximation SPM orders k for Example (13 - 17) when $M = 1, c = 0.5$.

An illustration of the maximumresidual error curves corresponding to Example (13 - 17) is given in Fig. 3. Again, it can be seen from this figure that the residual errors decrease sharply with an increase in the order of SPM approximation and plateau at a certain level.

5. CONCLUSION

In this paperwe consider the application of perturbation techniques with spectral methods in the solution of unsteady boundary layer flows caused by an impulsively stretching sheet. The applicability of the proposed method, called spectral perturbation method (SPM), was tested, respectively, on systems of one, two and three previously reported nonlinear partial differential equations that model different versions of unsteady

boundary layer flow problems. A residual error analysis was conducted in order to assess the accuracy of the present method. Computational efficiency of the method is demonstrated by comparing with results obtained using the Keller-Box method. It was found that the proposed SPM is much faster than the Keller-Box method. Unlike other numerical methods the SPM solves a partial differential equation by only applying discretization in the space direction. It is this feature, together with the integration using spectral methods (which require only a few grid points to yield accurate solutions) that make the SPM computationally efficient. The numerical results presented in this study clearly demonstrate the potential of the SPM scheme for the simulation of discussed model equations with high efficiency and accuracy. We conclude that the SPM can be used as a practical way of solving unsteady boundary layer problems defined using the Williams and Rhyne (1980) transformation. In future studies it would be interesting to explore the use of this method in general non-similarity boundary layer flow problems.

ACKNOWLEDGEMENTS

This workwork is based on the research supported in part by the National Research Foundation of South Africa (Grant No: 85596)

REFERENCES

Ahmad, I., M. Sajid, T. Hayat and M. Ayub (2008). Unsteady axisymmetric flow of asecond-grade fluid over a radially stretchingsheet. *Computers and Mathematics with Applications 56*, 1352–1357.

Ali, A. and A. Mehmood (2008). Homotopyanalysis of unsteady boundary layer flow adjacent to permeable stretching surface in aporous medium. *Commun. Nonlinear Sci. Numer. Simulat.* 13, 340–349.

Ali, F., R. Nazar and N. Arifin (2010). Numericalsolutions of unsteady boundary layer flow dueto an impulsively stretching surface. *Journalof Applied Computer Science and Mathematics* 8(4), Suceava.

Canuto, C., M. Hussaini, A. Quarteroni and T. Zang (1988). *Spectral Methods in FluidDynamics*. Berlin: Springer-Verlag.

Cebeci, T. and P. Bradshaw (1984). *Physical andComputational Aspects of Convective HeatTransfer*. New Tork: Springer.

Govardhan, K. and N. Kishan (2012).Unsteady MHD Boundary Layer Flow of an IncompressibleMicropolar Fluid over a Stretching Sheet, *Journal of Applied Fluid Mechanics* 5(3), 23-28.

Hayat, T., M. Qasim and Z. Abbas (2010). Homotopy solution for the unsteady three-dimensional mhd flow and mass transfer ina porous space. *Commun. Nonlinear Sci. Numer. Simulat.* 15, 2375–2387.

Kumari, M. and G. Nath (2009). Analytical solution of unsteady three-dimensional MHD boundary layer flow and heat transfer dueto impulsively stretched plane surface. *Commun. Nonlinear Sci. Numer. Simulat.* 14,3339–3350.

Liao, S. (2006). An analytic solution of unsteadyboundary-layer flows caused by an impulsively stretching plate. *Commun. NonlinearSci. Numer. Simulat.* 11, 326–339.

Makukula, Z. and S. Motsa (2014). Spectral Homotopy Analysis Method for PDEs That Model the Unsteady Von Karman Swirling Flow. *Journal of Applied Fluid Mechanics*, 7*(4)*, 711-718

Mehmood, A., A. Ali and T. Shah (2008). Heattransfer analysis of unsteady boundary layerflow by homotopy analysis method. *Commun.Nonlinear Sci. Numer. Simulat.* 13, 902–912.

Mehmood, A., A. Ali, H. Takhar and T. Shah(2008). Unsteady three-dimensional MHD boundary-layer flow due to the impulsive motion of a stretching surface. *Acta Mech.* 199,241–249.

Nadeem, S., A. Hussain and M. Khan (2010). HAM solutions for boundary layer flow inthe region of the stagnation point towards astretching sheet. *Commun. Nonlinear Sci. Numer. Simulat.* 15, 475–481.

Nazar, R., N. Amin and I. Pop (2004). Unsteadyboundary layer flow due to stretching surfacein a rotating fluid. *Mech. Res. Commun.* 31,121–128.

Nazar, R., N. Amin, D. Filip and I. Pop (2004). Unsteady boundary layer flow in the region of the stagnation point on a stretchingsheet. *International Journal of EngineeringScience* 42, 1241–1253.

Sajid, M., I. Ahmad, T. Hayat and M. Ayub (2008). Series solution for unsteady axisymmetric flow and heat transfer over a radially stretching sheet. *Communications in Nonlinear Science and Numerical Simulation* 13,2193 – 2202.

Sajid, M., I. Ahmad, T. Hayat and M. Ayub (2009). Unsteady flow and heat transfer of a second grade fluid over a stretching sheet. *Communications in Nonlinear Science and Numerical Simulation* 14, 96 – 108.

Seshadri, R., N. Sreeshylan and G. Nath (2002). unsteady mixed convection flow in the stagnation region of a heated vertical plate dueto impulsive motion. *Int. J. Heat Mass Transfer 45*, 1345 – 1352.

Tan, Y. and S. Liao (2007). Series solution of three-dimensional unsteady laminar viscous flow due to a stretching surface in a rotating fluid. *Journal of Applied Mechanics* 74, 1011– 1018.

Trefethen, L. (2000). *Spectral Methods in MATLAB*. SIAM.

Williams, J. and T. Rhyne (1980). Boundary layerdevelopment on a wedge impulsively set intomotion. *SIAM J. Appl. Math. 38*, 215 – 224.

Xu, H. and I. Pop (2008). Homotopy analysis ofunsteady boundary-layer flow started impulsively from rest along a symmetric wedge. *Z.Angew. Math. Mech.* 88(6), 507 – 514.

Xu, H., S. Liao and I. Pop (2006). Series solutions of unsteady boundary layer flow of amicropolar fluid near the forward stagnationpoint of a plane surface. *Acta Mechanica* 184,87 – 101.